Letter

Viscoplastic sessile drop coalescence

Vanessa R. Kern,* Torstein Sæter, and Andreas Carlson†
Department of Mathematics, Mechanics Division, University of Oslo, Oslo 0316, Norway

(Received 3 April 2022; accepted 18 July 2022; published 12 August 2022)

The evolution of the liquid bridge formed between two coalescing sessile yield-stress drops is studied experimentally. Surprisingly, we find that the height of the bridge evolves similar to a Newtonian fluid as $h_0(t) \sim t$, before arresting at long time due the fluid's yield stress. From viscoplastic lubrication theory we find a model for the arrested interface shape based on the balance between capillary pressure and yield stress. We then solve numerically for this final arrested profile shape and find it to depend on the fluid's yield stress τ_y, the surface tension coefficient σ and the coalescence angle α, represented by a modified Bingham number. We also present a scaling argument for the bridge's temporal evolution using the length scale found from this arrested shape analysis and present a similarity solution for the spatial evolution of the liquid bridge.

DOI: 10.1103/PhysRevFluids.7.L081601

Yield-stress fluids only flow when subjected to a stress greater than their yield stress τ_y. We rely on yield-stress fluids. They allow us to squeeze toothpaste from tubes, lay mortar for bricks, plaster walls, and even paint. Much focus has been spent on yield-stress flows [1,2] with a growing interest in capillary flows such as surface spreading for inkjet printing and spray coating [3–7], viscous fingering [8], and the adhesion of pastes [9].

We focus here on the dynamics of sessile viscoplastic drop coalescence utilizing both side-view and bottom-view imaging as shown in Figs. 1(a) and 1(b). When two drops coalesce, a liquid bridge forms between them. Much emphasis has been placed on the evolution of this bridge for both free and sessile Newtonian drops [10–13]. For sessile drops, the growth of the bridge can be characterized by its width $r_0(t)$ as viewed from below and its height $h_0(t)$ as viewed from the side. The presence of a symmetry breaking substrate generates additional stress near the growing bridge where the coalescence angle α can drastically alter its temporal evolution [14].

For Newtonian drops many different coalescence regimes have been identified. For free drop coalescence, or $\alpha = 90^\circ$, the bridge grows as $h_0(t) \sim t^{0.5}$ when the coalescence is inertially dominated [12] and as $h_0(t) \sim t$ with corrections in the early time as $h_0(t) \sim t \ln t$ when viscously dominated [15]. Similarly for viscous sessile drops $h_0(t) \sim t$ [13,15] and $r_0(t) \sim t^{0.5}$ [16] before transitioning to a Tanner's-like spreading at long times [17,18]. Early time inertial to late time viscous crossover has also been found to depend on liquid properties and drop size [19].

Despite relevance in many motivating applications [20–22], far less is known about non-Newtonian coalescence. For polymeric fluids, recently the effects of elasticity have been considered, showing polymer stretching affects spatial self-similarity, but in low concentrations not temporal growth [23]. Other studies have shown new scaling laws for temporal bridge growth [24], transitions from inertial to visco-elastic regimes [25], effects of approach velocity during sessile coalescence [26], and considerations of power-law fluid coalescence [27]. When two yield-stress drops coalesce,

*vanesske@math.uio.no
†acarlson@math.uio.no

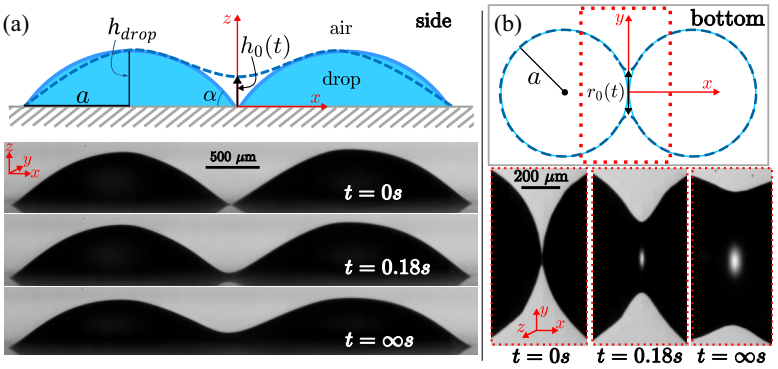

FIG. 1. Side (a) and bottom (b) view viscoplastic sessile drop coalescence with yield stress $\tau_y = 30\,\text{Pa}$. High speed imagery captures the coalescence event. Postcoalescence (b) the contact line spreads characterized by $r_0(t)$, and (a) the bridge grows characterized by its minima $h_0(t)$, before halting due to the drop's yield stress. The initial height of the drop h_{drop} and its footprint a are related through the coalescence angle α. Bottom and side view time sequences are presented from two different experiments with similar initial conditions.

their interface arrests before minimizing their surface energy. Arrested coalescence events have been previously observed for "jammed" interfaces in pickering emulsions [28] as well as for anisotropic colloids [29–31].

Here we find that the evolution of the liquid bridge formed during the coalescence of two sessile yield-stress drops behaves similarly to that of an $n = 1$ power-law fluid or a viscous Newtonian fluid in its temporal evolution $h_0(t) \sim t$. We propose a length scale based on the yield stress τ_y, surface tension σ, and aspect ratio h_{drop}/a to find a temporal scaling for the bridge evolution similar to that of a power-law fluid [27], and find the spatial evolution of the liquid bridge is self-similar [32]. These results are striking in that the effect of the yield stress appears to be subdominant to the dynamics of the bridge's evolution and that the yield-stress fluid's ability to have yielded, liquidlike and non-yielded, solidlike flow regions seems to play no role in the scaling of the bridge's evolution.

Experiment. Side- and bottom-view sessile coalescence events were imaged using a Photron Fastcam SA5 with a Nikon 200mm f/4 AF-D Macro lens and two teleconverters (Nikon 2x and 1.7x) resulting in resolutions of $\sim 6\,\mu$m/pixel. Further processing in Matlab using partial area subpixel edge detection techniques afforded resolutions below $6\,\mu$m/pixel [33,34]. Coalescence substrates were glass microscope slides (VWR Ca. 631-1550) rinsed with isopropanol (VWR Ca. 20922.364), plasma cleaned and kept in DI water until use. Immediately prior to use slides were blown dry with oil free compressed air. Coalescing drops were Carbopol 940 solutions with yield stresses varying from $\tau_y = 2\,\text{Pa}$ to 50 Pa measured using the stress growth test as shown in Fig. 2(b), details in the Supplemental Material [35]. Drop densities were assumed to be close to water $\rho \approx 1000\,\text{kg/m}^3$.

Only relatively spherically-cap shaped precoalescence sessile drops with aspect ratios $a/h_{\text{drop}} > 1.5$ and $\alpha < 45^\circ$ were considered. To minimize deviations from the spherical-cap shape, drops with footprints $a < 1\,\text{mm}$ were preferred [4]. When yield-stress drops spread on substrates, spreading arrests before drops minimize their surface energy as by the Young-Dupré equation $\sigma\cos(\alpha) = \sigma_{SV} - \sigma_{SL}$ [3]. Therefore for our experiments, the smallest obtainable initial coalescence angles α we expect are 6.5° to 34° for $\tau_y = 2\,\text{Pa}$ and 50 Pa, respectively [3,4,35]. Slides were plasma cleaned before each set of experiments to maintain a low substrate surface energy, thereby minimizing α. By knowing the initial drop size, approximate arrested angle, and footprint a at which spreading will cease, drops were simultaneously dispensed at known relative distances achieving both minimal α as well as contact line velocities below the initial bridge height velocity $dh_0(t)/dt$. Post coalescence, drops arrested within seconds rendering negligible evaporative losses.

Results. We frame our problem as a 2D flow parallel to the bridge justified by the small relative aspect ratio $h_0(t)/r_0(t) \ll 1$, and low film Reynolds number [12,15,35]. As the fluid has a yield

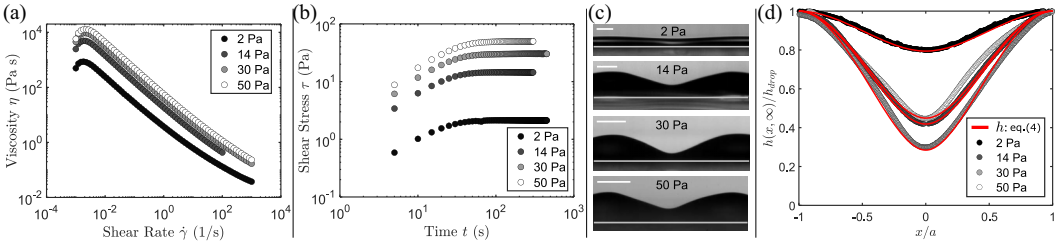

FIG. 2. (a), (b) Rheological data for Carbopol 940. A fit of the Herschel-Buckley model (2) recovers $n = [0.44, 0.4, 0.37, 0.37]$ and $K = [1.5, 4.0, 10.2, 14.9]$ Pa $\cdot$ s^n for yield stress $\tau_y = [2, 14, 30, 50]$ Pa samples respectively. (a) Measurement of viscosity against shear rate. (b) Measurement of yield stress using the constant oscillatory shear rate test. (c) Postcoalescence ($t = \infty$) final arrested shapes for increasing yield stress τ_y, each scale bar is 500 μm. For similar coalescence angles α, increasing τ_y decreases the arrested bridge height $h_0(\infty)$. Increases in α serve to increase the arrested bridge height, as shown for the 50 Pa case. (d) Comparison of the experimentally measured liquid/gas interfacial profiles $h(x,\infty)/h_{\text{drop}}$ (circles) against x/a with their corresponding numerical solutions (solid lines) obtained from a scaled (4), $\hat{h}(\hat{x})d^3\hat{h}(\hat{x})/d\hat{x}^3 = J/(h_{\text{drop}}/a)^3$, with boundary conditions $d\hat{h}(\hat{x})/d\hat{x} = 0$ at $(\hat{x} = -1, 0)$ and $\hat{h}(\hat{x} = -1) = 1$ for the experiments shown in (c).

stress τ_y, the system can be described using viscoplastic lubrication theory [3,36],

$$\frac{\partial h(x,t)}{\partial t} = \frac{n}{n+1}\left(\frac{1}{K}\right)^{\frac{1}{n}}\frac{\partial}{\partial x}\left(\left(\frac{nY(x,t)}{2n+1} - h\right)Y(x,t)^{\frac{1}{n}+1}\left|\frac{\partial P(x,t)}{\partial x}\right|^{\frac{1}{n}}\right),$$
$$\text{and } Y(x,t) = \max\left(0, h(x,t) - \tau_y\left|\frac{\partial P(x,t)}{\partial x}\right|^{-1}\right) \tag{1}$$

where $Y(x,t)$ represents the boundary between the yielded and non-yielded regions of the drop, $h(x,t)$ the liquid/gas interface, and $P(x,t)$ the capillary pressure. Here Carbopol is represented using the Herschel-Bulkley model with a stress τ versus shear rate $\dot{\gamma}$ dependency that can be expressed as

$$\tau = \tau_y + K\dot{\gamma}^n \text{ for } \tau \geqslant \tau_y, \tag{2}$$

where K and n are known as the consistency index and power-law index, respectively [37,38]. The fluid is yielded when $\tau > \tau_y$ and non-yielded when $\tau < \tau_y$ [39]. Expressed in terms of viscosity,

$$\eta = K|\dot{\gamma}|^{n-1} + \tau_y|\dot{\gamma}|^{-1}. \tag{3}$$

For our experiments $n = [0.44, 0.4, 0.37, 0.37]$ and $K = [1.5, 4.0, 10.2, 14.9]$Pa $\cdot$ s^n for yield stress $\tau_y = [2, 14, 30, 50]$ Pa samples, respectively. We see that $n < 1$ indicates a shear thinning flow as shown in Fig. 2(a). For lubrication theory to hold, one would expect for the coalescence angle α at which our experiment is constrained that the lubrication approximation would be inaccurate; however, this approximation has been shown to hold for α as large as $\alpha = 67^\circ$ [32].

It has been previously shown that due to the positively-charged nature of Carbopol's terminal group that Carbopol will have a non-negligible slip length on glass [40]. Considering that slip would modify (1) and could affect our experimental results, additional coalescence experiments presented in the Supplemental Material [35] were performed on waterproof sandpaper with a prewetted layer. We found that these experiments on sandpaper were qualitatively similar to those on glass, allowing us to reasonably assume the effects of slip did not influence our results.

Final arrested shape. Post Newtonian drop-drop coalescence, interfacial energies are minimized and the liquid/gas interface assumes a spherical-cap shape. However, post yield-stress drop-drop coalescence, the drop's bridge arrests at some fraction of its total height $h_0(\infty)/h_{\text{drop}}$, see Fig. 2(c).

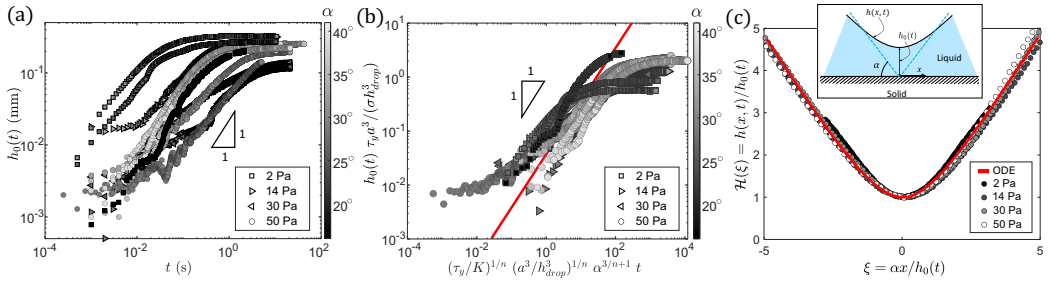

FIG. 3. Bridge evolution and self-similarity. (a) Unscaled bridge $h_0(t)$ evolution data. (b) Scaled bridge $h_0(t)$ evolution data. At early times the bridge growth is suggestive of $h_0(t) \sim t^n$ with $n \approx 0.4$ before evolving linearly as $h_0(t) \sim t$. At late times the growth ceases due to the yield stress τ_y. (c) Scaled drop interface $\mathcal{H}(\xi) = h(x,t)/h_0(t)$ against the similarity variable ξ from (5) with $\beta = 1$ in the linear regime of (d). The solid line is the numerically determined similarity solution obtained when $Y(x,t) \approx h(x,t)$ and $n = 1$ from (1), $\mathcal{H}(\xi) - \xi\mathcal{H}'(\xi) + 1/V(\mathcal{H}^3(\xi)\mathcal{H}'''(\xi))' = 0$ with one unknown parameter V and boundary conditions $\mathcal{H}(0) = 1$, $\mathcal{H}'(0) = \mathcal{H}'''(0) = 0$, $\mathcal{H}''(\infty) = 0$, and $\mathcal{H}'(\infty) = 1$ [32], $()' = d/d\xi$. Excellent agreement can be seen despite increasing τ_y.

From (1) we see that when $Y(x,t) = 0$ the yielded region of the drop vanishes. The shape of the arrested interface $h(x,\infty)$ can then be characterized by the nonlinear ordinary differential equation obtained from (1) in the limit $Y(x,\infty) \to 0$,

$$h(x,\infty)\frac{d^3h(x,\infty)}{dx^3} = \frac{\tau_y}{\sigma}. \tag{4}$$

Here the pressure $P(x,\infty)$ is approximated as the local interfacial curvature $\sigma\, d^2h(x,\infty)/dx^2$ with the small angle approximation and flow unidirectional towards the bridge $x = 0$. We numerically solve (4) as a system of first order ODEs in python using SciPy's "solve_bvp" function by prescribing the experimentally determined aspect ratio h_{drop}/a and Bingham number $J = \tau_y h_{\text{drop}}/\sigma$, scalings for the height $\hat{h}(\hat{x}) = h(x,\infty)/h_{\text{drop}}$ and length $\hat{x} = x/a$ and boundary conditions $d\hat{h}(\hat{x})/d\hat{x} = 0$ at $(\hat{x} = -1, 0)$ and $\hat{h}(\hat{x} = -1) = 1$, representing symmetry at $x = -a$, symmetry at the bridge $x = 0$, and the height of the drop, respectively. Here we note that the center of each drop relative to the symmetry plane at $x = 0$ remains near $x = |a|$ for all of our experiments.

Figure 2(d) shows the results of numerically integrating (4) with the y-axis rescaled compared with experimental data. We see good height profile agreement when the precoalesced drop shape is relatively spherically-capped, despite the fact that our model is 2D and ignores out of plane curvatures. In general, we find that initial deviations from a spherical-cap shape that are a byproduct of the initial deposition cause deviations in the final arrested profile. More details about this numerical solution as well as a comparison of numerically recovered versus experimentally measured final bridge heights $h_0(\infty)$ can be found in the Supplemental Material [35].

From the scaling of (4) we can see that a non-dimensional quantity in the form of the Bingham number modified by the aspect ratio $J/(h_{\text{drop}}/a)^3$ arises, begetting a new length scale $(h_{\text{drop}}/a)^3(\sigma/\tau_y)$. From this new length scale it can be seen that decreases in τ_y or increases in $\alpha \sim h_{\text{drop}}/a$ lead to an increase in the final arrested bridge height, recovering the intuition of a simple force balance shown in the Supplemental Material [35].

Temporal evolution. In Fig. 3(a) we use the bridge height $h_0(t)$ as a measure of the liquid bridge's temporal evolution and observe that α, τ_y, and K significantly affect the coalescence velocity and arrested bridge height. We observe for similar yield stresses τ_y that increasing α decreases the overall coalescence time and increases the final arrested bridge height $h_0(\infty)$ [35]. We also observe that for similar coalescence angles α that increasing the yield stress τ_y decreases the bridge velocity and the final arrested bridge height $h_0(\infty)$.

From (1) we can see that as $\tau_y \to 0$ or as $|\partial P(x,t)/\partial x| \gg \tau_y$ in regions of high interfacial curvature that $Y(x,t) \approx h(x,t)$, reducing (1) to the 2D lubrication equation for a power-law fluid [27,32,41]. Assuming a similarity solution of the form

$$\mathcal{H}(\xi) = \frac{h(x,t)}{vt^{\beta}}, \text{ with } \xi = \frac{\alpha x}{vt^{\beta}}, \tag{5}$$

and substituting into (1) we find that the liquid bridge should evolve in time as $h_0(t) \sim t^{\beta}$ with $\beta = n$ and with a scaling for the coalescence velocity $v \sim (\sigma/K)\alpha^{3+n}$. Using the length scale found in the previous section $(h_{\text{drop}}/a)^3(\sigma/\tau_y)$, a scaling for the coalescence time $\hat{t}$ can be written as

$$\hat{t} \sim \left(\frac{a^3\tau_y}{h_{\text{drop}}^3 K}\right)^{1/n} \alpha^{3/n+1} t. \tag{6}$$

It has been previously shown that both shear-thinning and yield-stress fluids in extensional rather than shear flow can behave similarly to constant viscosity Newtonian fluids [42]. Here we see a similar effect. Despite scanning a large parameter space, it can be seen from Fig. 3(a) that for the majority of the bridge's temporal evolution $\beta \neq n \approx 0.4$ but instead $\beta \approx 1$, indicating that the shear-thinning properties of the fluid appear to be subdominant for the majority of the dynamics of the growing liquid bridge and could be indicative of a flow of approximately constant shear rate and therefore constant viscosity. Similarly in the radial direction, the drop's advancing contact line spreads as $r_0(t) \sim t^{0.5}$ before transitioning to a long-time relaxation as $r_0(t) \sim t^{0.1}$ similar to Tanner's spreading law [18], shown in the Supplemental Material [35], supporting the idea of a flow of nearly constant viscosity.

The results of rescaling the data using (6) are shown in Fig. 3(b). As not all experiments are perfectly spherically-cap shaped initially, error inherently exists in the determination of the drop's aspect ratio h_{drop}/a and, consequently, coalescence angle α. However, despite these uncertainties, scaling in this fashion does group the data around a collapsed linear regime and suggest the existence of an early time regime of power-law growth where $\beta = n$, though this early time regime remains inconclusive as it occurs outside the temporal resolution of most of our experiments.

Due to similarities in the temporal evolution of the liquid bridge with $n = 1$ and $h_0(t) \sim t$ for the majority of the dynamics, we are then tempted to seek a similar universal rescaling and similarity solution using $n = 1$. For times $\hat{t}$ in the linear region of Fig. 3(b), we expect that the interface $h(x,t)$ should collapse onto a self-similar shape for all coalescence angles α and yield stresses τ_y, and by rescaling our data with the similarity variables of (5) with $\beta = 1$ we find that in this linear regime for varying yield stress a self-similar collapse of the liquid bridge's spatial evolution in time does occur as presented in Fig. 3(c). Comparing this collapse with the numerically calculated similarity solution from (1) with $Y(x,t) \approx h(x,t)$ and $n = 1$ shows excellent agreement, implying that for this system liquid-bridge evolutions across varying yield stresses are indeed self-similar and can be collapsed [32,41].

Discussion. Here we present a look at the sessile drop coalescence of viscoplastic drops. Surprisingly we find that the effect of the yield stress on the evolution dynamics is subdominant to the bridge evolution and that the majority of the bridge's evolution scales as a viscous, constant viscosity fluid or power-law fluid with $n = 1$, $h_0(t) \sim t$. At early times the data suggests the bridge's evolution may scale as a power-law fluid $h_0(t) \sim t^n$ with $n \approx 0.4$ for our Carbopol solutions, though this scaling remains inconclusive as it falls mostly outside the temporal resolution of our experiments. We postulate this reduction in the viscoplastic lubrication equations (1) to that of a power-law fluid can be explained for regions of rapidly changing interfacial curvature such as in the vicinity of $h_0(t)$.

We also find that both the yield stress τ_y and coalescence angle α affect the fractional height $h_0(\infty)/h_{\text{drop}}$ at which the evolving bridge arrests, and that the arrested interface shape can be described by the balance between the capillary pressure gradient and the fluid's yield stress. Lastly, we find a scaling that captures the spatial self-similarity in the bridge's evolution across multiple

yield stresses τ_y and coalescence angles α during the linear bridge evolution regime $n = 1$, and show that the bridge adopts a self-similar shape.

Here only experiments where drops were reasonably spherical-cap shaped were considered. These conditions, however, only represent a small set of cases for the coalescence of sessile yield-stress drops that can easily adopt highly nonspherical cap shapes [4]. It would then be interesting for future study to include drops with highly nonuniform initial liquid/gas interfacial curvatures and potentially larger initial coalescence angles α.

Acknowledgments. The authors sincerely thank an anonymous reviewer for their valuable comments and gratefully acknowledge the financial support of the Research Council of Norway through the program NANO2021, Project No. 301138.

[1] P. Coussot, Yield stress fluid flows: A review of experimental data, J. Non-Newtonian Fluid Mech. **211**, 31 (2014).
[2] N. J. Balmforth, I. A. Frigaard, and G. Ovarlez, Yielding to stress: recent developments in viscoplastic fluid mechanics, Annu. Rev. Fluid Mech. **46**, 121 (2014).
[3] M. Jalaal, B. Stoeber, and N. J. Balmforth, Spreading of viscoplastic droplets, J. Fluid Mech. **914**, A21 (2021).
[4] G. Martouzet, L. Jørgensen, Y. Pelet, A.-L. Biance, and C. Barentin, Dynamic arrest during the spreading of a yield stress fluid drop, Phys. Rev. Fluids **6**, 044006 (2021).
[5] M. Jalaal, C. Seyfert, B. Stoeber, and N. Balmforth, Gel-controlled droplet spreading, J. Fluid Mech. **837**, 115 (2018).
[6] M. Jalaal, C. Seyfert, and J. H. Snoeijer, Capillary ripples in thin viscous films, J. Fluid Mech. **880**, 430 (2019).
[7] R. de Ruiter, L. Royon, J. H. Snoeijer, and P. Brunet, Drop spreading and gelation of thermoresponsive polymers, Soft Matter **14**, 3096 (2018).
[8] A. Lindner, P. Coussot, and D. Bonn, Viscous Fingering in a Yield Stress Fluid, Phys. Rev. Lett. **85**, 314 (2000).
[9] Q. Barral, G. Ovarlez, X. Chateau, J. Boujlel, B. Rabideau, and P. Coussot, Adhesion of yield stress fluids, Soft Matter **6**, 1343 (2010).
[10] A. Menchaca-Rocha, A. Martínez-Dávalos, R. Nunez, S. Popinet, and S. Zaleski, Coalescence of liquid drops by surface tension, Phys. Rev. E **63**, 046309 (2001).
[11] S. Thoroddsen, K. Takehara, and T. Etoh, The coalescence speed of a pendent and a sessile drop, J. Fluid Mech. **527**, 85 (2005).
[12] L. Duchemin, J. Eggers, and C. Josserand, Inviscid coalescence of drops, J. Fluid Mech. **487**, 167 (2003).
[13] D. G. A. L. Aarts, H. N. W. Lekkerkerker, H. Guo, G. H. Wegdam, and D. Bonn, Hydrodynamics of Droplet Coalescence, Phys. Rev. Lett. **95**, 164503 (2005).
[14] A. Eddi, K. G. Winkels, and J. H. Snoeijer, Influence of Droplet Geometry on the Coalescence of Low Viscosity Drops, Phys. Rev. Lett. **111**, 144502 (2013).
[15] J. Eggers, J. R. Lister, and H. A. Stone, Coalescence of liquid drops, J. Fluid Mech. **401**, 293 (1999).
[16] W. D. Ristenpart, P. M. McCalla, R. V. Roy, and H. A. Stone, Coalescence of Spreading Droplets on a Wettable Substrate, Phys. Rev. Lett. **97**, 064501 (2006).
[17] D. Bonn, J. Eggers, J. Indekeu, J. Meunier, and E. Rolley, Wetting and spreading, Rev. Mod. Phys. **81**, 739 (2009).
[18] L. Tanner, The spreading of silicone oil drops on horizontal surfaces, J. Phys. D **12**, 1473 (1979).
[19] J. D. Paulsen, J. C. Burton, and S. R. Nagel, Viscous to Inertial Crossover in Liquid Drop Coalescence, Phys. Rev. Lett. **106**, 114501 (2011).
[20] V. Carrier and A. Colin, Coalescence in draining foams, Langmuir **19**, 4535 (2003).
[21] S. Tcholakova, N. D. Denkov, I. B. Ivanov, and B. Campbell, Coalescence stability of emulsions containing globular milk proteins, Adv. Colloid Interface Sci. **123-126**, 259 (2006).

[22] K. Mahdi, R. Gheshlaghi, G. Zahedi, and A. Lohi, Characterization and modeling of a crude oil desalting plant by a statistically designed approach, Journal of Petroleum Science and Engineering **61**, 116 (2008).
[23] P. J. Dekker, M. A. Hack, W. Tewes, C. Datt, A. Bouillant, and J. H. Snoeijer, When Elasticity Affects Drop Coalescence, Phys. Rev. Lett. **128**, 028004 (2022).
[24] S. C. Varma, A. Saha, S. Mukherjee, A. Bandopadhyay, A. Kumar, and S. Chakraborty, Universality in coalescence of polymeric fluids, Soft Matter **16**, 10921 (2020).
[25] S. C. Varma, A. Saha, and A. Kumar, Coalescence of polymeric sessile drops on a partially wettable substrate, Phys. Fluids **33**, 123101 (2021).
[26] V. S. Sivasankar, S. A. Etha, D. R. Hines, and S. Das, Coalescence of microscopic polymeric drops: Effect of drop impact velocities, Langmuir **37**, 13512 (2021).
[27] H. Chen, X. Pan, Q. Nie, Q. Ma, H. Fang, and Z. Yin, Probing the coalescence of non-Newtonian droplets on a substrate, Phys. Fluids **34**, 032109 (2022).
[28] A. B. Pawar, M. Caggioni, R. Ergun, R. W. Hartel, and P. T. Spicer, Arrested coalescence in pickering emulsions, Soft Matter **7**, 7710 (2011).
[29] A. B. Pawar, M. Caggioni, R. W. Hartel, and P. T. Spicer, Arrested coalescence of viscoelastic droplets with internal microstructure, Faraday Discuss. **158**, 341 (2012).
[30] D. J. Kraft, W. S. Vlug, C. M. van Kats, A. van Blaaderen, A. Imhof, and W. K. Kegel, Self-assembly of colloids with liquid protrusions, J. Am. Chem. Soc. **131**, 1182 (2009).
[31] S. Sacanna and D. J. Pine, Shape-anisotropic colloids: Building blocks for complex assemblies, Curr. Opin. Colloid Interface Sci. **16**, 96 (2011).
[32] J. F. Hernández-Sánchez, L. A. Lubbers, A. Eddi, and J. H. Snoeijer, Symmetric and Asymmetric Coalescence of Drops on a Substrate, Phys. Rev. Lett. **109**, 184502 (2012).
[33] A. Trujillo-Pino, K. Krissian, M. Alemán-Flores, and D. Santana-Cedrés, Accurate subpixel edge location based on partial area effect, Image and Vision Computing **31**, 72 (2013).
[34] A. Trujillo-Pino, Accurate subpixel edge location, https://www.mathworks.com/matlabcentral/fileexchange/48908-accurate-subpixel-edge-location, MATLAB Central File Exchange (2019).
[35] See Supplemental Material at http://link.aps.org/supplemental/10.1103/PhysRevFluids.7.L081601 for detailed rheological data.
[36] N. J. Balmforth, Viscoplastic asymptotics and other analytical methods, in *Lectures on Visco-Plastic Fluid Mechanics* (Springer, Cham, 2019) pp. 41–82.
[37] M. Shafiei, M. Balhoff, and N. W. Hayman, Chemical and microstructural controls on viscoplasticity in carbopol hydrogel, Polymer **139**, 44 (2018).
[38] N. J. Balmforth, A. Burbidge, R. Craster, J. Salzig, and A. Shen, Visco-plastic models of isothermal lava domes, J. Fluid Mech. **403**, 37 (2000).
[39] J. Boujlel and P. Coussot, Measuring the surface tension of yield stress fluids, Soft Matter **9**, 5898 (2013).
[40] M. Jalaal, N. J. Balmforth, and B. Stoeber, Slip of spreading viscoplastic droplets, Langmuir **31**, 12071 (2015).
[41] A. Oron, S. H. Davis, and S. G. Bankoff, Long-scale evolution of thin liquid films, Rev. Mod. Phys. **69**, 931 (1997).
[42] M. Aytouna, J. Paredes, N. Shahidzadeh-Bonn, S. Moulinet, C. Wagner, Y. Amarouchene, J. Eggers, and D. Bonn, Drop Formation in Non-Newtonian Fluids, Phys. Rev. Lett. **110**, 034501 (2013).